In the present study, dPasFHV without p53C′ induced the autophagic cell death of GICs, suggestting Pas to play a critical role in the induction of autophagy. Autophagy is a cellular pathway involved in protein and organelle degradation [25] and frequently activated in tumor cells following treatment with chemotherapeutic drugs [26,27] or γ-irradiation [28]. Autophagy is a catabolic process involving the degradation of the components of a cell by its own lysosomal machinery and a major mechanism by which a starving cell reallocates nutrients from unnecessary processes to more essential processes [31]. Recent studies showed that GICs contributes to the radioresistance of GBM with the induction of autophagy [34,35]. The induction of authophagy in GICs treated with dPasFHV-p53C′ may protect against apoptotic cell death. Although GICs are capable of escaping cell death by autophagy when treated with existing chemotherapeutic drugs, cells treated with dPasFHV-p53C′ and dPasFHV showed autophagic cell death. Chloroquine, used for the treatment of malaria, arrests the autophagy pathway by disrupting the cellular lysosomal function and altering the fusion of autophagosomes with lysosomes, resulting in the accumulation of autophagosomes and induction of autophagic cell death [31]. Pas enhances the internalization efficiency of arginine-rich CPPs including poly-arginine and FHV peptides [18]. This effect may be due to the disruption of macropinosomal and endosomal membranes in which cell-penetrating peptides are entrapped and prevention of the subsequent fusion with lysosomes and degradation in lysosomes [18]. These results suggest that dPasFHV may induce autophagic cell death of GICs by preventing the fusion of autophagosomes with lysosomes (Fig. 8).

5. Conclusion

The present results showed that dPasFHV-p53C′ and dPasFHV induced autophagic cell death of GICs. dPasFHV-p53C′ reduced tumor mass in mice transplanted with GICs. The present results suggest peptide transduction therapy using dPasFHV-p53C′ to be a method for the treatment of GBM.

Acknowledgments

We thank N. Maeda for technical assistance. This work was supported by a Grant-in-aid for Scientific Research from the Ministry of Education, Culture, Sports, Science and Technology of Japan and by the Japan Society for the Promotion of Science (JSPS) through its "Funding Program for Next Generation World-Leading Researchers".

Appendix A. Supplementary data

Supplementary data related to this article can be found at http://dx.doi.org/10.1016/j.biomaterials.2012.09.003.

References

[1] Van Meir EG, Hadjipanayis CG, Norden AD, Shu HK, Wen PY, Olson JJ. Exciting new advances in neuro-oncology: the avenue to a cure for malignant glioma. CA Cancer J Clin 2010;60:166–93.
[2] Kohsaka S, Wang L, Yachi K, Mahabir R, Narita T, Itoh T, et al. STAT3 inhibition overcomes temozolomide resistance in glioblastoma by downregulating MGMT expression. Mol Cancer Ther 2012;11:1289–99.
[3] Singh SK, Clarke ID, Hide T, Dirks PB. Cancer stem cells in nervous system tumors. Oncogene 2004;23:7267–73.
[4] Singh SK, Clarke ID, Terasaki M, Bonn VE, Hawkins C, Squire J, et al. Identification of a cancer stem cell in human brain tumors. Cancer Res 2003;63:5821–8.
[5] Singh SK, Hawkins C, Clarke ID, Squire JA, Bayani J, Hide T, et al. Identification of human brain tumor initiating cells. Nature 2004;432:396–401.
[6] Beier H, Hau P, Proescholdt M, Lohmeier A, Wischhusen J, Oefner PJ, et al. CD133(+) and CD133(-) glioblastoma-derived cancer stem cells show differential growth characteristics and molecular profiles. Cancer Res 2007;67:4010–5.
[7] Eyler CE, Rich JN. Survival of the fittest: cancer stem cells in therapeutic resistance and angiogenesis. J Clin Oncol 2008;26:2839–45.
[8] Bode AM, Dong Z. Post-translational modification of p53 in tumorigenesis. Nat Rev Cancer 2004;4:793–805.
[9] Olsson A, Manzl C, Strasser A, Villunger A. How important are post-translational modifications in p53 for selectivity in target-gene transcription and tumor suppression? Cell Death Differ 2007;14:1561–75.
[10] Hupp TR, Sparks A, Lane DP. Small peptides activate the latent sequence-specific DNA binding function of p53. Cell 1995;83:237–45.
[11] Snyder EL, Meade BR, Saenz CC, Dowdy SF. Treatment of terminal peritoneal carcinomatosis by a transducible p53-activating peptide. PLoS Biol 2004;2:E36.
[12] Joliot A, Prochiantz A. Transduction peptides: from technology to physiology. Nat Cell Biol 2004;6:189–96.
[13] Gupta B, Levchenko TS, Torchilin VP. Intracellular delivery of large molecules and small particles by cell-penetrating proteins and peptides. Adv Drug Deliv Rev 2005;57:637–51.
[14] Wadia JS, Dowdy SF. Transmembrane delivery of protein and peptide drugs by TAT-mediated transduction in the treatment of cancer. Adv Drug Deliv Rev 2005;57:579–96.
[15] Snyder EL, Saenz CC, Denicourt C, Meade BR, Cui XS, Kaplan IM, et al. Enhanced targeting and killing of tumor cells expressing the CXC chemokine receptor 4 by transducible anticancer peptides. Cancer Res 2005;65:10646–50.
[16] Wadia JS, Stan RV, Dowdy SF. Transducible TAT-HA fusogenic peptide enhances escape of TAT-fusion proteins after lipid raft macropinocytosis. Nat Med 2004;10:310–5.
[17] Yasuda Y, Kageyama T, Akamine A, Shibata M, Kominami E, Uchiyama Y, et al. Characterization of new fluorogenic substrates for the rapid and sensitive assay of cathepsin E and cathepsin D. J Biochem 1999;125:1137–43.
[18] Takayama K, Nakase I, Michiue H, Takeuchi T, Tomizawa K, Matsui H, et al. Enhanced intracellular delivery using arginine-rich peptides by the addition of penetration accelerating sequences (Pas). J Control Release 2009;138:128–33.
[19] Araki D, Takayama K, Inoue M, Watanabe T, Kumon H, Futaki S, et al. Cell-penetrating D-isomer peptides of p53 C-terminus: long-term inhibitory effect on the growth of bladder cancer. Urology 2010;75:813–9.
[20] Takezaki T, Hide T, Takanaga H, Nakamura H, Kuratsu J, Kondo T. Essential role of the Hedgehog signaling pathway in human glioma-initiating cells. Cancer Sci 2011;102:1306–12.
[21] Kondo T. Brain cancer stem-like cells. Eur J Cancer 2006;42:1237–42.
[22] Higuchi Y, Shiraki N, Yamane K, Qin Z, Mochitate K, Araki K, et al. Synthesized basement membranes direct the differentiation of mouse embryonic stem cells into pancreatic lineages. J Cell Sci 2010;123:2733–42.
[23] Wu HY, Tomizawa K, Oda Y, Wei FY, Lu YF, Matsushita M, et al. Critical role of calpain-mediated cleavage of calcineurin in excitotoxic neurodegeneration. J Biol Chem 2004;279:4929–40.
[24] Tomizawa K, Sunada S, Lu YF, Oda Y, Kinuta M, Ohshima T, et al. Cophosphorylation of amphiphysin I and dynamin I by Cdk5 regulates clathrin-mediated endocytosis of synaptic vesicles. J Cell Biol 2003;163:813–24.
[25] Klionsky DJ, Emr SD. Autophagy as a regulated pathway of cellular degradation. Science 2000;290:1717–21.
[26] Kim EH, Sohn S, Kwon HJ, Kim SU, Kim MJ, Lee SJ, et al. Sodium selenite induces superoxide-mediated mitochondrial damage and subsequent autophagic cell death in malignant glioma cells. Cancer Res 2007;67:6314–24.
[27] Abedin MJ, Wang D, McDonnell MA, Lehmann U, Kelekar A. Autophagy delays apoptotic death in breast cancer cells following DNA damage. Cell Death Differ 2007;14:500–10.
[28] Apel A, Herr I, Schwarz H, Rodemann HP, Mayer A. Blocked autophagy sensitizes resistant carcinoma cells to radiation therapy. Cancer Res 2008;68:1485–94.
[29] Kabeya Y, Mizushima N, Ueno T, Yamamoto A, Kirisako T, Noda T, et al. LC3, a mammalian homologue of yeast Apg8p, is localized in autophagosome membranes after processing. EMBO J 2000;19:5720–8.
[30] Mizushima N, Yoshimori T. How to interpret LC3 immunoblotting. Autophagy 2007;3:542–5.
[31] Espina V, Liotta LA. What is the malignant nature of human ductal carcinoma in situ? Nat Rev Cancer 2011;11:68–75.
[32] Maher EA, Furnari FB, Bachoo RM, Rowitch DH, Louis DN, Cavenee WK, et al. Malignant glioma: genetics and biology of a grave matter. Genes Dev 2001;15:1311–33.
[33] Bao S, Wu Q, McLendon RE, Hao Y, Shi Q, Hjelmeland AB, et al. Glioma stem cells promote radioresistance by preferential activation of the DNA damage response. Nature 2006;444:756–60.
[34] Lomonaco SL, Finniss S, Xiang C, Decarvalho A, Umansky F, Kalkanis SN, et al. The induction of autophagy by gamma-radiation contributes to the radioresistance of glioma stem cells. Int J Cancer 2009;125:717–22.
[35] Lomonaco SL, Finniss S, Xiang C, Lee HK, Jiang W, Lemke N, et al. Cilengitide induces autophagy-mediated cell death in glioma cells. Neuro Oncol 2011;13:857–65.

THE JOURNAL OF BIOLOGICAL CHEMISTRY VOL. 287, NO. 27, pp. 23236–23245, June 29, 2012
Published in the U.S.A.

Anks4b, a Novel Target of HNF4α Protein, Interacts with GRP78 Protein and Regulates Endoplasmic Reticulum Stress-induced Apoptosis in Pancreatic β-Cells*[S]

Received for publication, April 3, 2012, and in revised form, May 11, 2012 Published, JBC Papers in Press, May 15, 2012, DOI 10.1074/jbc.M112.368779

Yoshifumi Sato[‡1], Mitsutoki Hatta[‡1], Md. Fazlul Karim[‡1,2], Tomohiro Sawa[§¶], Fan-Yan Wei[‖], Shoki Sato[‡], Mark A. Magnuson[**], Frank J. Gonzalez[‡‡], Kazuhito Tomizawa[‖], Takaaki Akaike[§], Tatsuya Yoshizawa[‡], and Kazuya Yamagata[‡3]

From the Departments of [‡]Medical Biochemistry and [§]Microbiology, Faculty of Life Sciences, Kumamoto University, Kumamoto 860-8556, Japan, [¶]PRESTO, Japan Science and Technology Agency (JST), 4-1-8 Honcho Kawaguchi, Saitama 332-001, Japan, the [‖]Department of Molecular Physiology, Faculty of Life Sciences, Kumamoto University, Kumamoto, Japan the [**]Department of Molecular Physiology and Biophysics, Vanderbilt University School of Medicine, Nashville, Tennessee 37232, and the [‡‡]Laboratory of Metabolism, NCI, National Institutes of Health, Bethesda, Maryland 20814

Background: Target genes of HNF4α in β-cells are largely unknown.
Results: Expression of Anks4b is decreased in the βHNF4α KO islets. HNF4α activates Anks4b promoter activity. Anks4b binds to GRP78 and regulates sensitivity to ER stress.
Conclusion: HNF4α novel target gene, *Anks4b*, regulates the susceptibility of β-cells to ER stress.
Significance: Anks4b is a novel molecule involved in ER stress.

Mutations of the *HNF4A* gene cause a form of maturity-onset diabetes of the young (MODY1) that is characterized by impairment of pancreatic β-cell function. HNF4α is a transcription factor belonging to the nuclear receptor superfamily (NR2A1), but its target genes in pancreatic β-cells are largely unknown. Here, we report that ankyrin repeat and sterile α motif domain containing 4b (Anks4b) is a target of HNF4α in pancreatic β-cells. Expression of Anks4b was decreased in both βHNF4α KO islets and HNF4α knockdown MIN6 β-cells, and HNF4α activated Anks4b promoter activity. Anks4b bound to glucose-regulated protein 78 (GRP78), a major endoplasmic reticulum (ER) chaperone protein, and overexpression of Anks4b enhanced the ER stress response and ER stress-associated apoptosis of MIN6 cells. Conversely, suppression of Anks4b reduced β-cell susceptibility to ER stress-induced apoptosis. These results indicate that Anks4b is a HNF4α target gene that regulates ER stress in β-cells by interacting with GRP78, thus suggesting that HNF4α is involved in maintenance of the ER.

Hepatocyte nuclear factor (HNF)[4] 4α, a transcription factor belonging to the nuclear receptor superfamily (NR2A1), is expressed in the liver, pancreas, kidney, and intestine (1, 2). HNF4α has multiple functional domains, including the N-terminal A/B domain associated with the transactivation domain (AF-1), a DNA binding C domain, a functionally complex E domain that forms a ligand binding domain, a dimerization interface and transactivation domain (AF-2), and an F domain with a negative regulatory function (3, 4). HNF4α predominantly binds to a 6-bp repeat (AGGTCA) with a 1-bp spacer (mainly A) called direct repeat (DR1).

Maturity-onset diabetes of the young (MODY) is a genetically heterogeneous monogenic disorder that accounts for 2–5% of type 2 diabetes (5). We discovered that mutations of the human *HNF4A* gene cause a particular form of MODY known as MODY1 (6). The primary pathogenesis of MODY1 involves dysfunction of pancreatic β-cells (5). In addition, it has been shown that targeted disruption of HNF4α in pancreatic β-cells leads to defective insulin secretion in mice (7, 8). These findings have demonstrated that HNF4α has an important role in β-cells.

In the liver, HNF4α plays a critical role in nutrient transport and metabolism by regulating numerous target genes, including phosphoenolpyruvate carboxykinase (*PCK1*), glucose-6-phosphatase (*G6PC*), apolipoprotein AII (*APOA2*), and microsomal triglyceride transfer protein (*MTTP*) (9, 10). In contrast, we have little information about the target genes of HNF4α in pancreatic β-cells. Previous *in vitro* studies have suggested that

* This work was supported by a grant-in-aid for scientific research (B), a grant-in-aid for scientific research (S), a grant-in-aid for scientific research in innovative areas, a grant from the Ministry of Health Labour and Welfare, a grant from Takeda Science Foundation, a grant from Novo Nordisk Insulin Research Foundation, a grant from Banyu Life Science Foundation International, and a grant from Japan Diabetes Foundation.

[S] This article contains supplemental Tables 1 and 2 and supplemental Figs. 1–8.

[1] These authors contributed equally to this work.
[2] Supported by a scholarship from the International Priority Graduate Programs Advanced Graduate Courses for International Students, Ministry of Education, Culture, Sports, Science, and Technology in Japan.
[3] To whom correspondence should be addressed. Fax: 81-96-364-6940; E-mail: k-yamaga@kumamoto-u.ac.jp.

[4] The abbreviations used are: HNF, hepatocyte nuclear factor; MODY, Maturity-onset diabetes of the young; ER, endoplasmic reticulum; Anks4b, ankyrin repeat and sterile α motif domain containing 4b; TG, thapsigargin; CHOP, C/EBP homologous protein; C/EBP, CCAAT-enhancer-binding protein; BiP, binding immunoglobulin protein; ESI-Q-TOF, electrospray mass ionization-quadrupole-time-of-flight; KD, knockdown; FL, full-length; MUT, mutant.

HNF4α regulates the expression of pancreatic β-cell genes involved in glucose metabolism, such as insulin (*INS*), solute carrier family 2 (*SLC2A2*), and *HNF1A* (11). However, the expression of these genes was unchanged in the islets of β-cell-specific HNF4α knock-out (βHNF4α KO) mice (7, 8), indicating that such genes are not targets of HNF4α *in vivo*, at least in β-cells.

In the present study, we investigated the mRNA expression profile of βHNF4α KO mice and found that ankyrin repeat and sterile α motif domain containing 4b/harmonin-interacting, ankyrin repeat-containing protein (Anks4b/Harp) is a target of HNF4α in β-cells. We also demonstrated that Anks4b interacts with glucose-regulated protein 78 (GRP78), a major chaperone protein that protects cells from endoplasmic reticulum (ER) stress *in vitro* and *in vivo*. Gain- and loss-of-function studies of Anks4b revealed that it regulates sensitivity to thapsigargin (TG)-induced ER stress and apoptosis in MIN6 β-cell line. Our results suggest that HNF4α plays an important role in the regulation of ER stress and apoptosis in pancreatic β-cells.

EXPERIMENTAL PROCEDURES

Microarray Expression Profiling and HNF4α Motif Scan—Mice were maintained on a 12-h light/12-h dark cycle and allowed free access to food and water. All animal experiments were conducted according to the guidelines of the Institutional Animal Committee of Kumamoto University. Pancreatic islets were isolated from 45-week-old female βHNF4α KO mice (n = 5) and control flox/flox mice (n = 5) by collagenase digestion (12). Total RNA was prepared from the isolated islets with an RNeasy micro kit (Qiagen) according to the manufacturer's instructions, and its quality was confirmed by using an Agilent 2100 Bioanalyzer (Agilent Technologies, Palo Alto, CA). DNA microarray analysis was performed by the Kurabo GeneChip custom analysis service with GeneChip mouse genome 430 2.0 array (Affymetrix Inc., Santa Clara, CA). For identification of potential HNF4α binding sites, 5 kb of the promoter sequence upstream of the transcriptional start site was retrieved from the University of California Santa Cruz Genome Browser, and the sequence was analyzed by using the Transcription Element Search System (TESS) and the HNF4 Motif Finder generated by Sladek and colleagues (38).

Quantitative RT-PCR—Total RNA was extracted using an RNeasy micro kit (catalog number 74004, Qiagen, Valencia, CA) or Sepasol-RNA I super reagent (Nacalai Tesque, Kyoto, Japan). Then 1 μg of total RNA was used to synthesize first-strand cDNA with a PrimeScript RT reagent kit and gDNA Eraser (RR047A, TaKaRa Bio Inc., Shiga, Japan) according to the manufacturer's instructions. Quantitative real-time PCR was performed using SYBR *Premix Ex Taq* II (RR820A, TaKaRa) in an ABI 7300 thermal cycler (Applied Biosystems, Foster City, CA). The specific primers employed are shown in supplemental Table 1. Relative expression of each gene was normalized to that of TATA-binding protein.

Cell Lines and Culture—The MIN6 pancreatic β-cell line was cultured in Dulbecco's modified Eagle's medium (DMEM) containing 25 mM glucose, 15% fetal bovine serum, 0.1% penicillin/streptomycin, and 50 μM 2-mercaptoethanol at 37 °C under 5% CO_2, 95% air (13). HEK293, HeLa, and COS-7 cells were purchased from the American Type Culture Collection (ATCC) and were cultured in DMEM containing 2.5 mM glucose, 10% fetal bovine serum, and 0.02% penicillin/streptomycin.

Western Blotting—Cells were lysed in radioimmunoprecipitation assay buffer (50 mM Tris-HCl (pH 8.0), 150 mM NaCl, 0.1% SDS, 1% Nonidet P-40, 5 mM EDTA, 0.5% sodium deoxycholate, 20 μg/ml Na_3VO_4, 10 mM NaF, 1 mM PMSF, 2 mM DTT, and protease inhibitor mixture (1/100)) from Nacalai Tesque. Total protein was separated by SDS-polyacrylamide gel electrophoresis, transferred to a polyvinylidene fluoride (PVDF) membrane (Immobilon-P; Millipore, Bedford, MA), and probed with primary antibodies. After incubation with the secondary antibodies, the proteins were visualized using Chemi-Lumi One Super (Nacalai Tesque) and a LAS-1000 imaging system (Fuji Film, Tokyo, Japan). The primary antibodies used in this study were as follows: anti-HNF4α (1:1000) (H1415; Perseus Proteomics, Tokyo, Japan), anti-β-actin (1:2000) (A5441; Sigma-Aldrich), anti-harmonin (SAB250188; Sigma-Aldrich) (1:1000), anti-cleaved caspase-3 (Asp-175) (1:1000) (antibody 9661, Cell Signaling), and anti-GRP78 (1:1000) (sc-1051, Santa Cruz Biotechnology or antibody 4332, Cell Signaling).

Anti-Anks4b antiserum was generated by using a peptide that formed the central region of mouse Anks4b protein (amino acid residues 147–344). The nucleotide sequence of the peptide was amplified by PCR using a pair of primers (5′-CGGATCCCCATGAAAGAGTGCGAACGGCTT-3′ and 5′-CGGATCCCCTTACCATTCTACTTCTTCTTC-3′), and then it was subcloned into the pET28C+ vector. After expression in *Escherichia coli* BL21 (DE3), the His-tagged peptide was purified with His binding resin (Novagen) according to the manufacturer's instructions and dialyzed in a buffer containing 20 mM Tris-HCl (pH 8.0) and 500 mM NaCl. Subsequently, this peptide was used to inoculate rabbits for the production of anti-Anks4b antiserum.

Transient Transfection and Luciferase Reporter Assay—The mouse Anks4b promoter containing a putative HNF4α binding site was amplified by PCR using a pair of primers (5′-AGTGGTCATTGCCATGGTTGGT-3′ and 5′-AGGTAGGAGTCTTTGTCTAGGC-3′), and then it was subcloned into the pGL3 basic reporter (Promega). Transcription binding sites were altered by PCR-based mutagenesis to produce an HNF4α binding site mutant (GAACGGGGGCC) and an HNF1α binding site mutant (CTGACCGGCCAG). CD1b-HNF4α is a dominant negative mutant of HNF4α lacking the AF-2 activation domain (3). As described previously (14), the CD1b mutation was introduced by PCR into pcDNA3-HNF4α7 (kindly provided by Dr. Toshiya Tanaka, Tokyo University). The pcDNA3.1-wild-type (WT)-HNF1α and pcDNA3.1-P291fsinsC-HNF1α expression plasmids have been described previously (15). MIN6 cells or HEK293 cells (3×10^5 cells each) were seeded into 24-well plates at 18 h before transfection. Transient transfection was performed using Lipofectamine 2000 (Invitrogen) or X-treme GENE (Roche Applied Science) according to the manufacturer's instructions. At 24 h after transfection, luciferase activity was measured by using a Dual-Luciferase reporter assay system (Promega).

EMSA—A nuclear extract of MIN6 cells was prepared as described previously (16). Then 5 μg of the nuclear extract was incubated with ^{32}P-radiolabeled oligonucleotides containing the HNF4α or HNF1α binding sequence in a mixture containing 10 mM Tris-HCl (pH 7.5), 1% Ficoll, 70 mM KCl, 30 mg/ml BSA, 4.8% glycerol, and 100 μg/ml poly(dI-dC). Next, the DNA-protein complexes were resolved on 4% polyacrylamide gel in 0.5× Tris-borate-EDTA buffer at 120 V for 2 h, after which the dried gel was exposed to a phosphorimaging screen and analyzed with a BAS 2000 (Fuji Film). The oligonucleotide sequences were as follows: wild-type HNF4α binding site (5′-GGCCGGAGTGAACTTTGGCCTGGGGTGATA-3′); mutant HNF4α binding site (5′-GGCCGGAGTGAATGGGAGCCTGGGGTGATA-3′); wild-type HNF1α binding site (5′-CCCCGTCACTGATTAACCAGCCCTGTTGGA-3′); and mutant HNF1α binding site (5′-CCCCGTCACTGACCGGCCAGCCCTGTTGGA-3′). An anti-HNF1 antibody (H205, sc-8986) was used for the supershift assay.

Chromatin Immunoprecipitation—MIN6 cells were fixed in DMEM containing 1% formaldehyde for 10 min at room temperature, and then cross-linking was quenched by placing the cells in 200 mM glycine for 5 min at room temperature. The cells were incubated in Nonidet P-40 buffer (10 mM Tris-HCl (pH 8.0), 10 mM NaCl, 0.5% Nonidet P-40) for 5 min at room temperature and then lysed in SDS lysis buffer (50 mM Tris-HCl (pH 8.0), 1% SDS, 10 mM EDTA) followed by 5-fold dilution in ChIP dilution buffer (50 mM Tris-HCl (pH 8.0), 167 mM NaCl, 1.1% Triton X-100, and 0.11% sodium deoxycholate). Sonication was performed with a Sonifier 150 (Branson). Soluble sheared chromatin (20 μg) was incubated overnight at 4 °C with magnetic beads (Invitrogen Dynabeads protein G) bound to 2 μg of anti-HNF4α antibody (Santa Cruz Biotechnology sc-6556), anti-RNA polymerase *II* monoclonal antibody (Active Motif), or control IgG (Cell Signaling Technology antibody 2729) followed by sequential washing with low salt radioimmunoprecipitation assay buffer (50 mM Tris-HCl (pH 8.0), 150 mM NaCl, 1 mM EDTA, 0.1% SDS, 1% Triton X-100, and 0.1% sodium deoxycholate), high salt radioimmunoprecipitation assay buffer (50 mM Tris-HCl (pH 8.0), 500 mM NaCl, 1 mM EDTA, 0.1% SDS, 1% Triton X-100, and 0.1% sodium deoxycholate), wash buffer (50 mM Hepes-KOH (pH 7.5), 500 mM LiCl, 1 mM EDTA, 1% Nonidet P-40, and 0.7% sodium deoxycholate), and Tris-EDTA. Then immune complexes were eluted from the magnetic beads by incubation with ChIP direct elution buffer (50 mM Tris-HCl (pH 8.0), 10 mM EDTA, and 1% SDS) for 20 min at 65 °C. For reverse cross-linking, the eluate was incubated overnight at 65 °C, and then DNA fragments were purified by using a PCR purification kit (Qiagen). PCR was performed to identify Anks4b promoter fragments in the immunoprecipitated DNA using a pair of primers (5′-TTCACCACACTCATGACACACC-3′ and 5′-AGGTAGGAGTCTTTGTCTAGGC-3′).

GST Pulldown Assay—Mouse Anks4b cDNA was amplified by PCR using a pair of primers (5′-CGGATCCCCATGTCTACCCGCTATCACCAA-3′ and 5′-CGGATCCTTAGAGGCTGGTGTCAACCAACT-3′) and was subcloned into the pGEX4T2 vector (GE Healthcare). Anks4b deletion mutants (N-Anks4b (amino acid residues 1–126), M-Anks4b (amino acid residues 127–345), and C-Anks4b (amino acid residues 346–423)) were also generated by PCR and subcloned into the pGEX4T3 vector (GE Healthcare). GST-Anks4b proteins were expressed in *E. coli* BL21 (DE3) and purified with glutathione-Sepharose 4B beads (GE Healthcare). GST or GST fusion proteins (20 μg) immobilized on glutathione-Sepharose beads were incubated with 500 μg of mouse liver lysate. After binding overnight at 4 °C, the beads were washed with lysis buffer containing 10 mM Tris-HCl (pH 7.4), 150 mM NaCl, 1% Nonidet P-40, 1 mM EDTA, 10 mM NaF, 10 mM $Na_4P_2O_7$, 1 mM PMSF, and protease inhibitor mixture (Nacalai Tesque). Then the bound proteins were separated by SDS-PAGE.

Proteomic Identification of Anks4b-interacting Proteins—Silver-stained gels were subjected to in-gel digestion followed by extraction of peptides and proteomic analysis by LC-MS/MS. Gel digestion and peptide extraction were performed as reported previously (17). The peptide samples thus obtained were analyzed in an ESI-Q-TOF tandem mass spectrometer (6510; Agilent) with an HPLC chip-MS system, consisting of a nano pump (G2226; Agilent) with a four-channel microvacuum degasser (G1379B; Agilent), a microfluidic chip cube (G4240; Agilent), a capillary pump (G1376A; Agilent) with degasser (G1379B; Agilent), and an autosampler with thermostat (G1377A; Agilent). All modules were controlled by MassHunter software (version B.02.00; Agilent). A microfluidic reverse-phase-HPLC chip (Zorbax 300SB-C18; 5-μm particle size, 75-mm inner diameter, and 43 mm in length) was used for separation of peptides. The nano pump was employed to generate gradient nano flow at 600 nl/min, with the mobile phase being 0.1% formic acid in MS-grade water (solvent A) and 0.1% formic acid in acetonitrile (solvent B). The gradient was 5–75% solvent B over 9 min. A capillary pump was used to load samples with a mobile phase of 0.1% formic acid at 4 μl/min. The Agilent ESI-Q-TOF was operated in the positive ionization mode (ESI+), with an ionization voltage of 1,850 V and a fragmentor voltage of 175 V at 300 °C. Fragmentation of protonated molecular ions was conducted in the auto-MS/MS mode, starting with a collision energy voltage of 3 V that was increased by 3.7 V per 100 Da. The selected m/z ranges were 300–2,400 Da in the MS mode and 59–3,000 Da in the MS/MS mode. The data output consisted of one full mass spectrum (with three fragmentation patterns per spectrum) every 250 ms. The three highest peaks of each MS spectrum were selected for fragmentation. Mass lists were created in the form of Mascot generic files and were used as the input for Mascot MS/MS ion searches of the National Center for Biotechnology Information nonredundant (NCBI nr) database using the Matrix Science Web server Mascot version 2.2. Default search parameters were as follows: enzyme, trypsin; maximum missed cleavage, 1; variable modifications, carbamidomethyl (Cys); peptide tolerance, ± 1.2 Da; MS/MS tolerance, ± 0.6 Da; peptide charge, 2+ and 3+; instrument, ESI-Q-TOF. For positive identification, the result of ($-10 \times \log (p)$) could not exceed the significance threshold ($p < 0.05$).

Immunoprecipitation—Mouse Anks4b cDNA was amplified by PCR using a pair of primers (5′-CGGATCCCCATGTCTACCCGCTATCACCAA-3′ and 5′-CGGATCCTTAGAGGCTGGTGTCAACCAACT-3′) and was subcloned in-frame

into the pcDNA3-HA and pcDNA3-FLAG expression vectors. The GRP78 expression vector (pCMV-BiP-Myc-KDEL-wt) was a gift from Dr. Ron Prywes (Addgene plasmid 27164). After transfection into COS-7 cells, the cells were lysed in immunoprecipitation buffer (20 mM Tris-HCl (pH 7.4), 175 mM NaCl, 2.5 mM $MgCl_2$, 0.05% Nonidet P-40, 1 mM PMSF, and protease inhibitor mixture (Nacalai Tesque)) and incubated on ice for 30 min. Then 700 μg of cell lysate and FLAG tag antibody beads (Wako) were mixed and stirred at 4 °C for 18 h. After washing with immunoprecipitation buffer, proteins were eluted by using DYKDDDDK peptide (Wako). A sample of the eluate and 2% of the cell lysate (from before processing) were subjected to Western blotting analysis.

Immunocytochemistry—Both the pcDNA3-HA-Anks4b and the pCMV-BiP-Myc-KDEL-wt vectors were transfected into HeLa, COS-7, and MIN6 cells with X-treme GENE (Roche Diagnostics) for 24 h. Then the cells were fixed in 10% neutralized formalin and permeabilized with 0.1% Triton X-100, 3% BSA/PBS. Monoclonal rat anti-HA antibody (1:400) (clone 3F10, Roche Applied Science) and mouse anti-c-Myc antibody (1:400) (Wako) were used as the primary antibodies, whereas Alexa Fluor 568 goat anti-rat IgG (Invitrogen) and Alexa Fluor 488 goat anti-mouse IgG (Invitrogen) were used as the secondary antibodies. Immunofluorescence was detected under a laser scanning confocal microscope (FV-1000, Olympus, Tokyo, Japan).

Retrovirus Infection—Mouse Anks4b and human HNF4α7 cDNAs were subcloned into the pMXs-puro retrovirus vector for overexpression (18). Specific shRNA sequences for mouse HNF4α (5′-CCAAGAGCTGCAGATTGAT-3′) and Anks4b (5′-GAAGAAGACTCATTTCCAA-3′) were designed using the Clontech RNAi target sequence selector. Oligonucleotides encoding shRNA were synthesized and cloned into the pSIREN-RetroQ retroviral shRNA expression vector (Clontech). Then the pMXs-Anks4b, pMXs-HNF4α7, and empty pMXs vectors were transfected into Plat-E cells using FuGENE6 (Roche Applied Science, Mannheim, Germany). For knockdown experiments, transfection was done with pSIREN-RetroQ-Anks4b, pSIREN-RetroQ-HNF4α, and the negative control pSIREN-RetroQ vector. MIN6 cells were infected with the retroviruses and selected by incubation with puromycin (5 μg/ml) (12).

Flow Cytometric Analysis—An annexin V-FITC apoptosis detection kit (BioVision Research Products, Mountain View, CA) was used for the apoptosis assay according to the manufacturer's instructions. MIN6 cells were cultured in DMEM for 30 h with or without 1 μM thapsigargin (Nacalai Tesque). After incubation in trypsin/EDTA for 10 min at 37 °C, cells were centrifuged at 6,000 rpm for 10 min. The pellet was resuspended in 1×resuspension buffer, and the cells were stained with annexin V-FITC antibody. After incubation for 5 min at room temperature in the dark, stained cells were analyzed using a FACSCalibur (BD Biosciences) and FlowJo software (Tomy Digital Biology, Tokyo, Japan).

Statistical Analysis—Statistical analyses were performed using Statview J-5.0 software (SAS Institute, Cary, NC). The significance of differences was assessed with the unpaired *t* test, and $p < 0.05$ was considered to indicate statistical significance.

RESULTS

Anks4b Is a Novel Target of HNF4α—To identify target genes of HNF4α in pancreatic β-cells, DNA microarray analysis was performed using islets from βHNF4α KO mice and control mice. Body weight and blood glucose levels were similar for these two strains of mice (body weight was 32.7 ± 1.7 g ($n = 5$) *versus* 34.1 ± 1.9 g ($n = 5$) and random blood glucose was 128 ± 27 mg/dl ($n = 5$) *versus* 114 ± 24 mg/dl ($n = 5$) for βHNF4α KO *versus* control mice). Microarray analysis identified 56 up-regulated genes (signal log ratio ≥2) and 100 down-regulated genes (signal log ratio ≤−1.5) in βHNF4α KO islets (supplemental Table 2). Expression of the majority of the genes known to be involved in glucose metabolism was unchanged. To validate these results, expression of mRNA for genes randomly chosen from both the down-regulated and the up-regulated groups was assessed by quantitative real-time PCR in an independent group of 12-week-old male mice. As a result, differential expression of most genes was confirmed (Fig. 1*A* and supplemental Fig. 1). Gupta *et al.* (19) reported that ST5, a regulator of ERK activation, is a direct target of HNF4α in β-cells. Expression of ST5 mRNA was reduced by 24.6% in βHNF4α KO islets (supplemental Fig. 2).

Next, we performed a computational scan of the *HNF4α* binding motif in the down-regulated genes. This identified 22 high affinity HNF4α binding sequences in the mouse promoter. In 3 out of 22 genes, the HNF4 motif was also conserved in the corresponding human genome. These three genes encoded *Anks4b*, guanylate cyclase 2c (*Gucy2c*), and peroxisome proliferator-activated receptor γ coactivator-1α (*Ppargc1a*). Quantitative real-time PCR analysis confirmed a significant decrease of Anks4b expression in the islets of 12-week-old βHNF4α KO mice (17.3% of the control level, $p < 0.01$) (Fig. 1*B*). In contrast, the reduction of Gucy2c mRNA expression was marginal (21.7% of the control level, $p = 0.06$), and *Ppargc1a* mRNA levels were unchanged. The difference of sex and age of mice or different detection systems might have contributed to the different results. To elucidate the direct effect of HNF4α on the expression of these three genes, we established MIN6 β-cells that stably expressed HNF4α-specific shRNA (HNF4α KD-MIN6) by retroviral infection. Suppression of endogenous HNF4α was confirmed at both the mRNA and the protein levels (Fig. 1*C*). Decreased expression of *Anks4b*, *Gucy2c*, and *Ppargc1a* was found in HNF4α KD-MIN6 cells (Fig. 1*D*). Because *Anks4b* gene expression was most markedly decreased in both βHNF4α KO islets and HNF4α KD-MIN6 cells (35.2% of the control level, $p < 0.001$), we focused on Anks4b for further investigation.

Screening of the promoter region of the mouse Anks4b gene by using a genomic databank revealed an HNF4α binding site (nucleotides −108 to −120 relative to the translation start codon when A is designated as +1). We cloned a 190-bp promoter region upstream of a luciferase reporter gene and co-expressed it with the HNF4α expression vector in HEK293 cells. Induction of HNF4α7 (an isoform expressed in pancreatic β-cells (4)) increased Anks4b promoter activity in a concentration-dependent manner (Fig. 2*A*), whereas overexpression of the HNF4α mutant lacking AF-2 had no effect (Fig. 2*B*). When

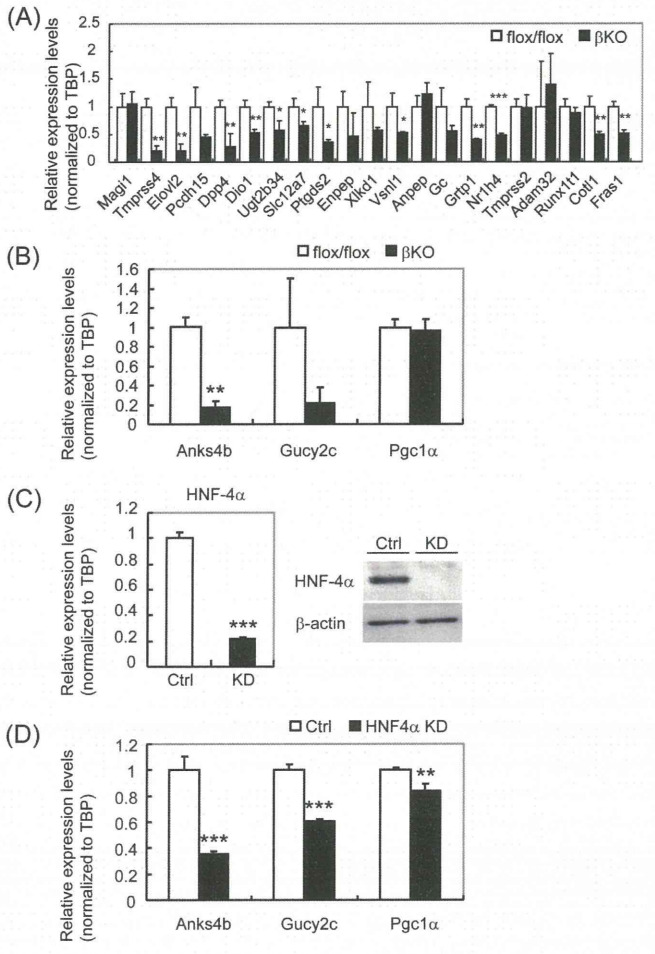

FIGURE 1. **Gene expression in the islets of βHNF4α KO mice and HNF4α knockdown MIN6 cells.** *A*, quantitative RT-PCR analysis of genes randomly chosen from those in supplemental Table 1 using flox/flox control (*white bar*) and βHNF4α KO islets (*black bar*, male, 12 week, $n = 4$). Expression of each gene was normalized for that of TATA-binding protein (*TBP*). *B*, expression of *Anks4b*, *Gucy2c*, and *Ppargc1a* in βHNF4α KO islets. Decreased expression of Anks4b was confirmed by quantitative RT-PCR. *C*, HNF4α mRNA (*left*) and HNF4α protein (*right*) in control (*Ctrl*, *white bar*) and HNF4α knockdown MIN6 cells (*KD*, *black bar*) were evaluated by quantitative PCR ($n = 4$) and Western blotting, respectively. β-Actin was used as the loading control. *D*, expression of *Anks4b*, *Gucy2c*, and *Ppargc1a* was significantly decreased in HNF4α KD-MIN6 cells. The mean ± S.D. for each group is shown (*, $p < 0.05$, **, $p < 0.01$, ***, $p < 0.001$).

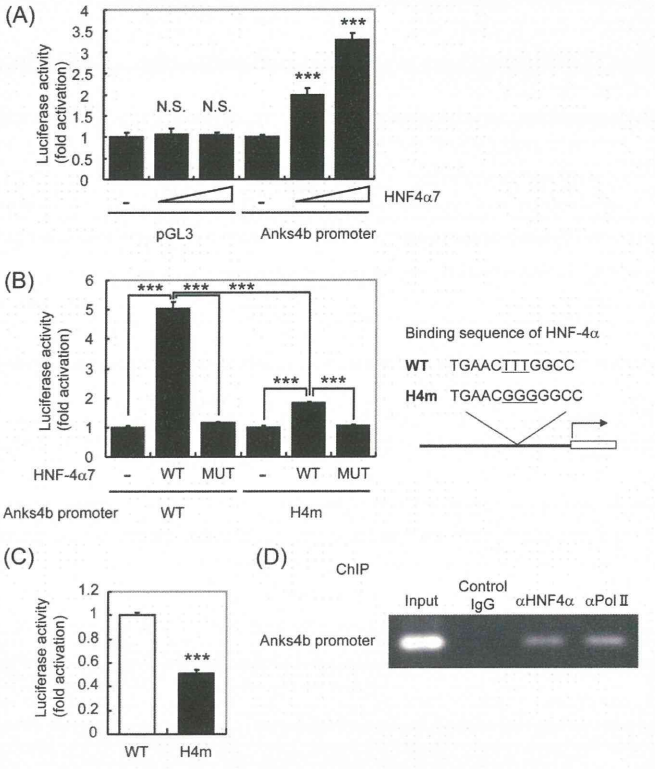

FIGURE 2. **Transcriptional regulation of Anks4b by HNF4α.** *A*, HEK293 cells were cotransfected with the pcDNA3-HNF4α7 expression vector (0–75 ng), as well as 50 ng of pGL3 basic or pGL3-Anks4b reporter and 25 ng of pRL-TK. *B*, HEK293 cells were cotransfected with 50 ng of pcDNA3-wild-type-HNF4α7 (WT) or pcDNA3-mutant (MUT) HNF4α7, as well as 50 ng of pGL3-Anks4b reporter (WT and MUT) and 25 ng of pRL-TK. *C*, MIN6 cells were transfected with pGL3-Anks4b reporter (WT and MUT) and 25 ng of pRL-TK. The mean ± S.D. for each group ($n = 3$) is shown (***, $p < 0.001$). *N.S.*, not significant. *D*, chromatin immunoprecipitation assay with MIN6 cells. Interaction of HNF4α with the promoter of Anks4b was observed. *αPol II*, RNA polymerase II antibody.

the putative HNF4α binding site in the Anks4b promoter was subjected to mutation (H4m), transcriptional activation by HNF4α7 was significantly reduced by 64.0% ($p < 0.001$) (Fig. 2*B*). Disruption of the HNF4α binding site was also associated with a 48.5% reduction of promoter activity in MIN6 cells ($p < 0.001$) (Fig. 2*C*). To assess the binding of HNF4α to the Anks4b promoter, a chromatin immunoprecipitation (ChIP) assay was performed using MIN6 cells. This assay revealed binding of HNF4α to the Anks4b promoter of MIN6 cells (Fig. 2*D*). Specific binding of HNF4α to the putative binding site was also demonstrated by the electrophoretic mobility shift assay (EMSA) (supplemental Fig. 3). Thus, both *in vivo* and *in vitro* data indicated that Anks4b is a direct target of HNF4α in β-cells.

HNF4α and HNF1α Synergistically Activate Transcription of Anks4b—HNF1α is a homeodomain-containing transcription factor that is also expressed in the liver, kidney, intestine, and pancreas (20). Mutation of the *HNF1A* gene causes another type of MODY known as MODY3 (21). In addition to the binding site for HNF4α, we also found an HNF1α binding consensus sequence in the Anks4b promoter (Fig. 3*A*). Therefore, we examined the role of HNF1α in Anks4b gene transcription. First, binding of HNF1α to the Anks4b gene was examined by EMSA with MIN6 nuclear extracts and a probe corresponding to the HNF1α binding site (Fig. 3*B*). The probe shifted after the addition of nuclear extracts (*lane 2*), and its binding was blocked by the addition of a 30-fold excess of unlabeled oligonucleotide (*lane 3*). Specificity of HNF1α binding was assessed by supershifting the DNA-HNF1α complex using HNF1α antibody (*lane 5*), indicating that HNF1α also binds directly to the Anks4b promoter. To examine the influence of HNF1α on Anks4b gene expression, we next performed a reporter gene assay. WT-HNF1α caused a dose-dependent increase of Anks4b promoter activity (Fig. 3*C*). Interestingly, Anks4b mRNA expression was decreased in HNF1α KO islets according to the results of DNA microarray analysis (22). Taken together, these results suggested that Anks4b is a target of

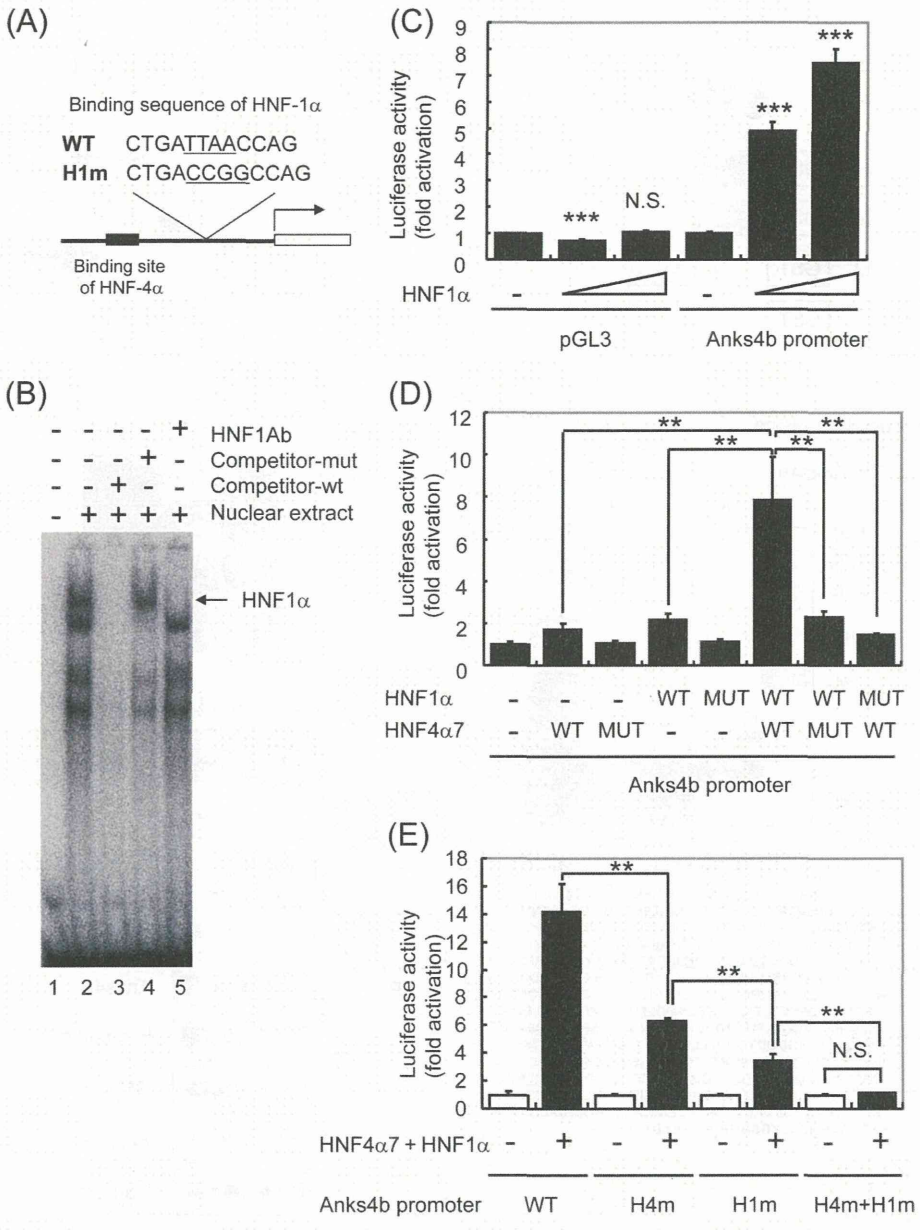

FIGURE 3. **Synergistic activation of Anks4b transcription by HNF4α and HNF1α.** *A*, DNA sequences of the promoter region of the mouse and human Anks4b genes. The putative HNF4α and HNF1α binding sites are shown. *B*, EMSA analysis of the HNF1α binding site in the Anks4b gene. DNA binding was tested using nuclear extracts from MIN6 cells. *C*, HEK293 cells were cotransfected with the pcDNA3.1-HNF1α expression vector (0–75 ng), as well as 50 ng of pGL3 basic or pGL3-Anks4b reporter and 25 ng of pRL-TK. *D*, HEK293 cells were cotransfected with 10 ng of pcDNA3.1-HNF1α (WT or MUT) and 10 ng of pcDNA3-HNF4α7 (WT or MUT), as well as 50 ng of pGL3-Anks4b reporter and 5 ng of pRL-TK. *E*, HEK293 cells were cotransfected with pcDNA3.1-HNF1α and pcDNA3-HNF4α7 as well as 50 ng of pGL3-Anks4b reporter (WT or MUT). *H4m*, mutation of the HNF4α binding site; *H1m*, mutation of the HNF1α binding site. *H4m+H1m*, mutation of both binding sites. The mean ± S.D. for each group ($n = 3$) is shown (**, $p < 0.01$, ***, $p < 0.001$). *N.S.*, not significant.

HNF1α as well as HNF4α. Because it has been reported that HNF4α and HNF1α cooperatively activate target genes that have binding sites for both HNFs in the promoter region (23, 24), we examined the influence on Anks4b gene expression of interaction between HNF4α and HNF1α. When an Anks4b reporter construct was cotransfected into HEK293 cells with 10 ng of HNF1α or HNF4α expression plasmid, the reporter gene was activated by 2.2- and 1.7-fold, respectively (Fig. 3*D*). In contrast, there was a dramatic increase of promoter activity (7.9-fold) when both constructs were cotransfected simultaneously (Fig. 3*D*). Mutation of either HNF1α or HNF4α markedly suppressed this response (Fig. 3*D*). Synergistic activation of Anks4b promoter activity was significantly suppressed by disruption of either the HNF4α binding site (H4m) or the HNF1α binding site (H1m), and activation was completely abolished by both H4m and H1m (Fig. 3*E*). Taken together, these results indicate that Anks4b promoter activity is synergistically regulated by both HNF4α and HNF1α.

Anks4b Interacts with GRP78 Both in Vitro and in Vivo—Anks4b is a scaffold protein with three ankyrin repeats and a sterile α motif domain that was identified as harmonin-interacting protein (25), although its function is completely

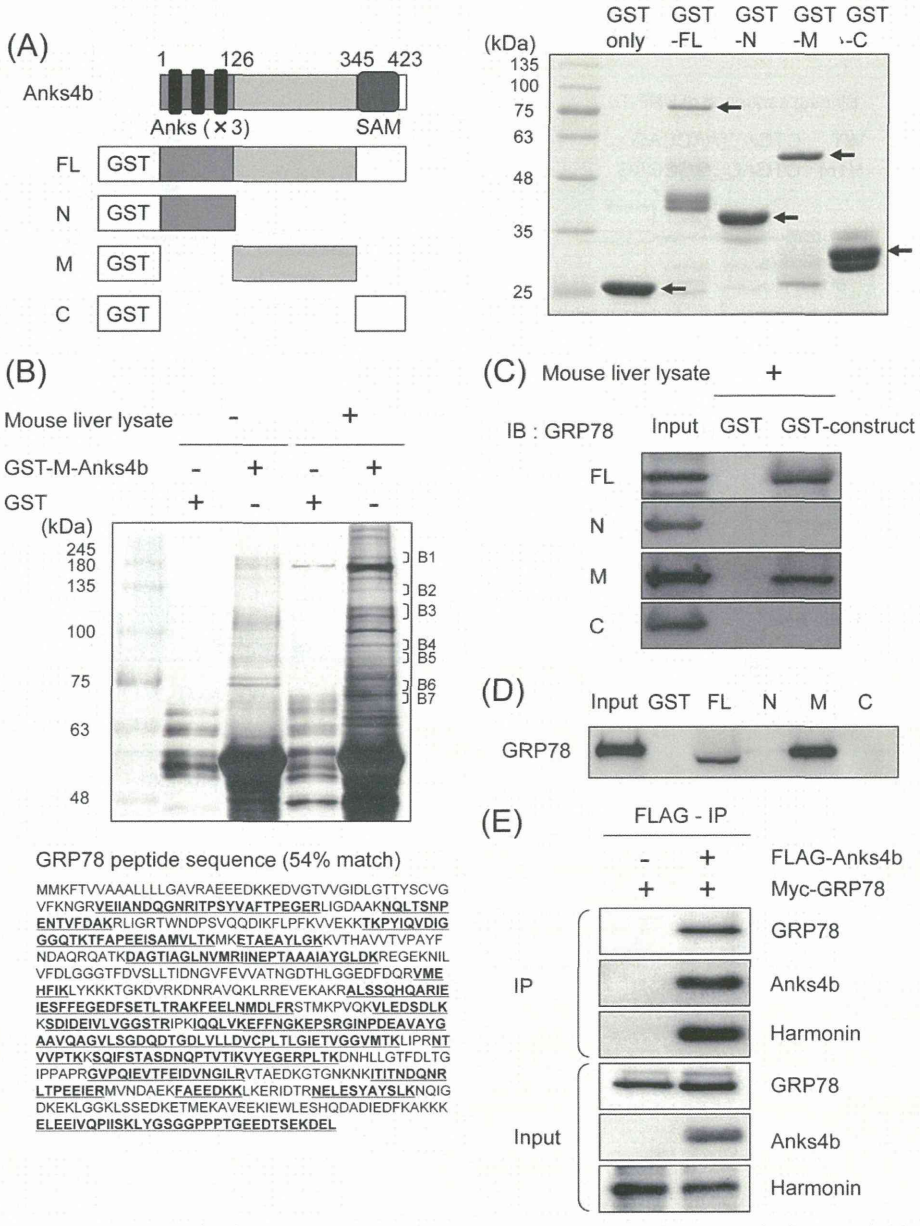

FIGURE 4. **Interaction of Anks4b and GRP78 *in vitro* and *in vivo*.** *A*, schematic representation of full-length Anks4b (*FL*) and deletion mutants of Anks4b (N-Anks4b (*N*), M-Anks4b (*M*), and C-Anks4b (*C*)) and expression of GST-Anks4b fusion proteins (Coomassie Brilliant Blue staining). *SAM*, sterile α motif. *B*, purification of proteins interacting with Anks4b. The GST pulldown assay using M-Anks4b was performed with mouse liver lysates. Eluted proteins were resolved by SDS-PAGE and then silver-stained. Seven regions (*B1–B7*) were excised for mass spectrometry. GRP78 residues were detected by mass spectrometry (*bold* and *underlined letters*). *C* and *D*, interaction of Anks4b and GRP78 *in vitro*. After the pulldown assay using mouse liver lysates (*C*) or MIN6 lysates (*D*), binding of GRP78 with FL- and M-Anks4b was detected by Western blotting (*IB*). *E*, interaction of Anks4b and GRP78 *in vivo*. COS-7 cells were transfected with the pCMV-Bip/GRP78-Myc-KDEL-wt or pCMV-Bip/GRP78-Myc-KDEL-wt and pcDNA3-FLAG-Anks4b expression vectors. Immunoprecipitation (*IP*) was performed with FLAG resin and 700 μg of COS-7 cell lysate.

unknown. To elucidate the role of Anks4b in β-cells, we searched for molecules that interacted with full-length Anks4b (FL) and with its deletion mutants (N-, M-, and C-Anks4b) (Fig. 4*A*) by performing a GST pulldown assay of mouse liver lysates (Fig. 4*B* and supplemental Fig. 4). We found a protein of ~75 kDa that specifically precipitated with GST-M-Anks4b (B6), and it was identified as GRP78/binding immunoglobulin protein (BiP) by mass spectrometry (Fig. 4*B*). GRP78 is an ER-localized chaperone protein that is induced by the unfolded protein response in response to ER stress (26, 27). Binding of GRP78 to GST-FL-Anks4b and GST-M-Anks4b, but not to GST, GST-N-Anks4b, or C-Anks4b, was confirmed by Western blotting using a specific antibody for GRP78 (Fig. 4*C*), suggesting that GRP78 bound to the middle region of Anks4b. GST pulldown experiments using MIN6 cell lysates also demonstrated binding of GRP78 to Anks4b (Fig. 4*D*).

Subsequently, we evaluated the interaction between Anks4b and GRP78 in cultured cells. COS-7 cells were transfected with the Myc-GRP78 expression plasmid alone or with Myc-GRP78 plus FLAG-tagged wild-type Anks4b expression plasmids, and

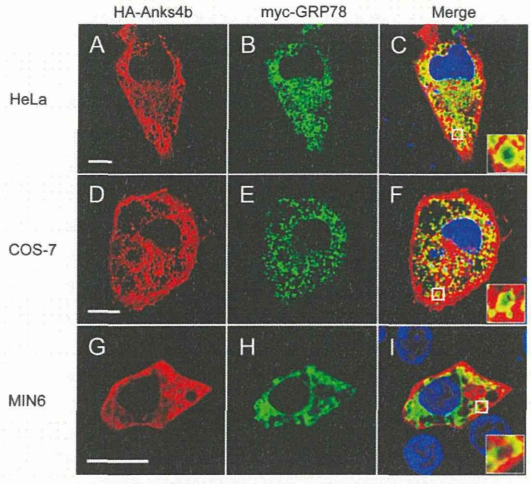

FIGURE 5. **Intracellular localization of Anks4b adjacent to the ER membrane.** *A–I*, HeLa (*A–C*), COS-7 (*D–F*), and MIN6 (*G–I*) cells were cotransfected with the pcDNA3-HA-Anks4b and pCMV-Bip/GRP78-Myc-KDEL-wt expression vectors. Cells were double-stained with anti-HA antibody (Alexa Fluor 563, *red*) and anti-Myc antibody (Alexa Fluor 488, *green*). DAPI (*blue*) was used for nuclear staining. *Insets* represent higher magnifications of the *boxed regions* in *C* (×18), *F* (×13), and *I* (×8). *Scale bar* = 10 μm.

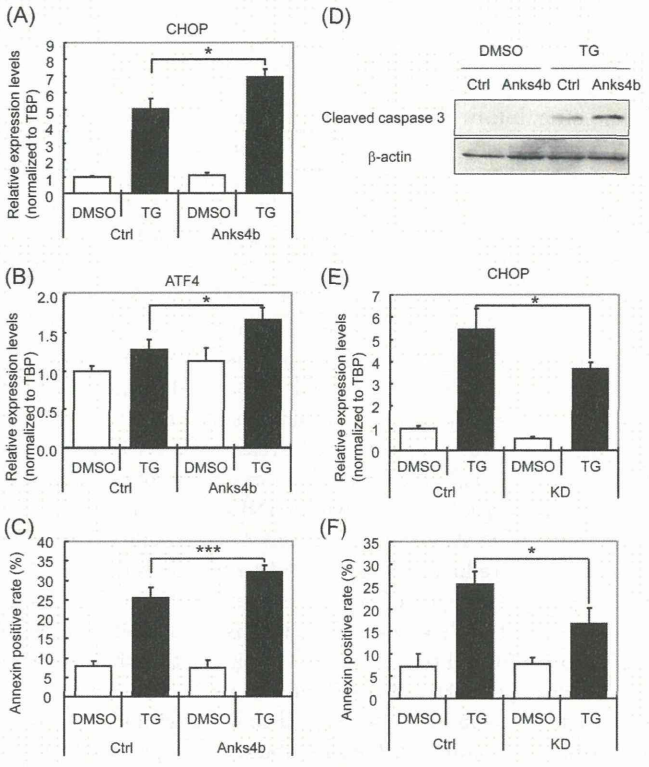

FIGURE 6. **Regulation of ER stress-mediated apoptosis by Anks4b.** *A* and *B*, MIN6 cells overexpressing Anks4b were cultured in the absence or presence of 1 μM thapsigargin for 20 h, and then quantitative RT-PCR was performed. *TBP*, TATA-binding protein. *DMSO*, dimethyl sulfoxide; *Ctrl*, control. *C*, MIN6 cells overexpressing Anks4b were cultured in the absence or presence of 1 μM thapsigargin for 30 h, and the percentage of annexin V-positive cells was analyzed by flow cytometry. *D*, Western blotting of cleaved caspase-3 after treatment with 1 μM thapsigargin for 20 h. *E*, Anks4b knockdown MIN6 cells were cultured for 20 h with 1 μM thapsigargin, and then quantitative RT-PCR was performed. *F*, annexin V-positive cells were analyzed after treatment of Anks4b knockdown MIN6 cells with 1 μM thapsigargin for 30 h. The mean ± S.D. for each group ($n = 4$) is shown (*, $p < 0.05$, **, $p < 0.01$, ***, $p < 0.001$).

cell lysates were immunoprecipitated with FLAG resin. As shown in Fig. 4*E*, FLAG-Anks4b was able to coimmunoprecipitate GRP78 as well as harmonin, a protein that was previously found to interact with Anks4b (25). These results indicated that Anks4b binds to GRP78 in cells.

Anks4b Colocalizes with GRP78 in the Endoplasmic Reticulum—We next investigated the intracellular localization of Anks4b. HA-tagged Anks4b and Myc-tagged GRP78 constructs were cotransfected into HeLa cells, and an immunofluorescence study was performed. HA staining (Anks4b, *red*) revealed a reticular pattern in the cytoplasm, but no signals were detected in the nucleus (Fig. 5*A*). Double staining for Anks4b and GRP78 (Myc, *green*) as a marker for the ER revealed that both signals were frequently colocalized (Fig. 5, *B* and *C*). In contrast, Anks4b staining did not overlap with MitoTracker, a specific marker for the mitochondria (supplemental Fig. 5). A similar staining pattern was also detected in COS-7 cells and MIN6 cells (Fig. 5, *D–I*). These findings were further evidence that Anks4b interacts with GRP78. Notably, Anks4b staining was detected at the periphery of the ER lumen (Fig. 5, *C*, *F*, and *I*, *inset*), suggesting that it was localized adjacent to the ER membrane.

Anks4b Regulates Apoptosis in Response to ER Stress—GRP78 is a major chaperone protein that protects cells from ER stress, and overexpression of GRP78 reduces ER stress-mediated apoptosis by attenuating the expression of C/EBP homologous protein (CHOP) (28, 29). Accordingly, detection of an interaction between Anks4b and GRP78 prompted us to investigate the role of Anks4b in both ER stress and apoptosis. TG causes ER stress by preventing calcium uptake from the cytoplasm into the ER (30), and treatment of MIN6 cells with 1 μM TG for 20 h increased the expression of the ER stress-related genes (ATF4, spliced XBP1, and CHOP) (data not shown). First, we examined the effect of Anks4b overexpression on MIN6 cells (supplemental Fig. 6). Anks4b overexpression did not affect CHOP gene expression in the absence of TG, but TG-induced CHOP expression was significantly increased (1.4-fold, $p < 0.05$) (Fig. 6*A*). TG-induced ATF4 expression was also significantly augmented in Anks4b-overexpressing MIN6 cells (1.3-fold, $p < 0.05$) (Fig. 6*B*). Furthermore, the number of annexin V-positive apoptotic cells was increased by overexpression of Anks4b (1.3-fold, $p < 0.001$) (Fig. 6*C*). Augmentation of apoptosis was also observed in MIN6 cells overexpressing HNF4α7 (supplemental Fig. 7). Activation of caspase-3 mediates the induction of apoptosis downstream of CHOP (31), and activated (cleaved) caspase-3 protein expression was increased when Anks4b-overexpessing MIN6 cells were treated with TG (Fig. 6*D*).

Next, we examined the effect of knockdown of Anks4b in MIN6 cells (supplemental Fig. 8). Suppression of endogenous Anks4b mRNA by shRNA in MIN6 (reduced to 40.5% of the control level) did not affect CHOP gene expression in the absence of TG, but TG-induced CHOP expression was significantly reduced by 32.1% ($p < 0.05$) (Fig. 6*E*). In addition, flow cytometric analysis using annexin V revealed that TG-induced apoptosis was also decreased by suppression of Anks4b (Fig. 6*F*). Collectively, these findings indicate that Anks4b promotes the induction of ER stress and apoptosis by TG in MIN6 cells.

DISCUSSION

HNF4α plays an important role in pancreatic β-cells, and mutation of this gene causes MODY1 (6). However, there has been little information available about the target genes of HNF4α in β-cells. We and others have previously reported that most of the genes involved in glucose metabolism, including *Slc2a2*, *Gck*, *Kcnj11*, *Abcc8*, and *Ins*, are not differentially expressed in βHNF4α KO islets (7, 8, 19). The present large scale expression profiling analysis also demonstrated that expression of genes known to be involved in insulin secretion was largely unchanged in HNF4α deficient islets. Like HNF4α, mutation of the HNF1α gene also causes a form of MODY (MODY3), which is characterized by β-cell dysfunction (21). Expression of many genes involved in insulin secretion, including *Slc2a2*, *Pklr*, and *Tmem27*, is decreased in HNF1α KO islets (22, 32, 33). Thus, the gene expression pattern of HNF4α KO islets differs markedly from that of HNF1α KO islets.

In the present study, we found that Anks4b gene expression was markedly reduced in both βHNF4α KO islets and HNF4α KD-MIN6 cells. Reporter gene assays and ChIP analysis demonstrated that HNF4α bound to a conserved HNF4 binding motif and activated transcription, thus indicating that Anks4b is a direct target of HNF4α in β-cells. In addition to the pancreatic islets, Anks4b is also expressed in the liver, kidney, small intestine, and colon (25). This distribution of expression is very similar to that of HNF4α, suggesting that HNF4α plays a role in Anks4b gene transcription in these tissues. Furthermore, we found that Anks4b gene expression was also regulated by HNF1α. Cotransfection of HNF4α and HNF1α dramatically stimulated promoter activity when compared with the sum of the effects of each transcription factor acting separately (Fig. 3*D*). Recently, Boj *et al.* (34) reported that HNF4α and HNF1α regulate common target genes through interdependent regulatory mechanisms. Although the mechanism of the functional interaction between HNF4α and HNF1α is still unclear, our results indicate that Anks4b gene expression is another example of such interdependent regulation.

Anks4b was originally identified as harmonin (the gene responsible for Usher deafness syndrome type 1C)-interacting protein, but its function is unknown. In this study, we showed that Anks4b binds to GRP78, a major ER chaperone protein. We also found that Anks4b knockdown significantly inhibited TG-induced CHOP expression and apoptosis in MIN6 cells, whereas Anks4b overexpression enhanced TG-induced CHOP expression and apoptosis, strongly suggesting a direct role of Anks4b in increasing the susceptibility of β-cells to ER stress and apoptosis. Investigation of Anks4b knock-out mice will improve our understanding of the role of this molecule in ER stress. Anks4b does not possess the canonical ER localization signal (35), so the molecular mechanism by which Anks4b binds to GRP78 and regulates ER stress warrants further investigation.

HNF4α plays an important role in a number of metabolic pathways, including those for gluconeogenesis, ureagenesis, fatty acid metabolism, and drug metabolism (36–38). Our finding that Anks4b is a target of HNF4α uncovers a new role for this transcription factor in regulating β-cell susceptibility to ER stress. ER stress is associated with β-cell apoptosis in common type 2 diabetes (39). Because reduced expression of Anks4b was associated with a decrease, rather than an increase, of ER stress and apoptosis, the significance of Anks4b in relation to the occurrence of MODY is unclear. However, recent genetic studies have shown that HNF4α has dual opposing roles in the β-cell during different periods of life. Although HNF4α deficiency results in diabetes in young adults (6), the same genetic defect occasionally causes hyperinsulinemic hypoglycemia at birth (40, 41). Further studies will need to address whether reduced Anks4b expression is responsible for the hypersecretion of β-cells early in life.

In conclusion, we identified Anks4b as a novel molecule that controls the susceptibility to ER stress-induced apoptosis. The ER is critical for the normal functioning of pancreatic β-cells, and ER stress-associated apoptosis is often a contributory factor to β-cell death in type 2 diabetes (39). Therefore, Anks4b may be a potential target for the treatment of diabetes associated with ER stress.

Acknowledgments—We thank Prof. J. Miyazaki (Osaka University) for the gift of MIN6 cells, Prof. T. Kitamura (Tokyo University) for providing the Plat-E cells and pMXs vector, and Dr. T. Tanaka (Tokyo University) for providing pcDNA3-HNF4α7 plasmid.

REFERENCES

1. Sladek, F. M., Zhong, W. M., Lai, E., and Darnell, J. E. (1990) Liver-enriched transcription factor HNF-4 is a novel member of the steroid hormone receptor superfamily. *Genes Dev.* **4,** 2353–2365
2. Nammo, T., Yamagata, K., Tanaka, T., Kodama, T., Sladek, F. M., Fukui, K., Katsube, F., Sato, Y., Miyagawa, J., and Shimomura, I. (2008) Expression of HNF-4α (MODY1), HNF-1β (MODY5), and HNF-1α (MODY3) proteins in the developing mouse pancreas. *Gene Expr. Patterns* **8,** 96–106
3. Hadzopoulou-Cladaras, M., Kistanova, E., Evagelopoulou, C., Zeng, S., Cladaras, C., and Ladias, J. A (1997) Functional domains of the nuclear receptor hepatocyte nuclear factor 4. *J. Biol. Chem.* **272,** 539–550
4. Ihara, A., Yamagata, K., Nammo, T., Miura, A., Yuan, M., Tanaka, T., Sladek, F. M., Matsuzawa, Y., Miyagawa, J., and Shimomura, I. (2005) Functional characterization of the HNF4α isoform (HNF4α8) expressed in pancreatic β-cells. *Biochem. Biophys. Res. Commun.* **329,** 984–990
5. Bell, G. I., and Polonsky, K. S. (2001) Diabetes mellitus and genetically programmed defects in β-cell function. *Nature* **414,** 788–791
6. Yamagata, K., Furuta, H., Oda, N., Kaisaki, P. J., Menzel, S., Cox, N. J., Fajans, S. S., Signorini, S., Stoffel, M., and Bell, G. I. (1996) Mutations in the hepatocyte nuclear factor-4α gene in maturity-onset diabetes of the young (MODY1) *Nature* **384,** 458–460
7. Miura, A., Yamagata, K., Kakei, M., Hatakeyama, H., Takahashi, N., Fukui, K., Nammo, T., Yoneda, K., Inoue, Y., Sladek, F. M., Magnuson, M. A., Kasai, H., Miyagawa, J., Gonzalez, F. J., and Shimomura, I. (2006) Hepatocyte nuclear factor-4α is essential for glucose-stimulated insulin secretion by pancreatic β-cells. *J. Biol. Chem.* **281,** 5246–5257
8. Gupta, R. K., Vatamaniuk, M. Z., Lee, C. S., Flaschen, R. C., Fulmer, J. T., Matschinsky, F. M., Duncan, S. A., and Kaestner, K. H. (2005) The MODY1 gene HNF-4α regulates selected genes involved in insulin secretion. *J. Clin. Invest.* **115,** 1006–1015
9. Hayhurst, G. P., Lee, Y. H., Lambert, G., Ward, J. M., and Gonzalez, F. J. (2001) Hepatocyte nuclear factor 4α (nuclear receptor 2A1) is essential for maintenance of hepatic gene expression and lipid homeostasis. *Mol. Cell Biol.* **21,** 1393–1403
10. Rhee, J., Inoue, Y., Yoon, J. C., Puigserver, P., Fan, M., Gonzalez, F. J., and Spiegelman, B. M. (2003) Regulation of hepatic fasting response by PPARγ coactivator-1α (PGC-1): requirement for hepatocyte nuclear factor 4α in gluconeogenesis. *Proc. Natl. Acad. Sci. U.S.A.* **100,** 4012–4017